

HIGH-SPEED PIN-TRAVELING WAVE PHOTODETECTOR BASED ON A SEMICONDUCTOR OPTICAL AMPLIFIER LAYER STACK ON SEMI-INSULATING InP SUBSTRATE

M. Nikoufard^{1,*}, F. S. Alaei Tabatabaei², and S. N. Ghafouri²

¹Department of Electrical Engineering, Faculty of Engineering, University of Kashan, Kashan, Iran

²Department of Electrical Engineering, South Tehran Branch, Islamic Azad University, Tehran, Iran

Abstract—We present a pin-Traveling wave Photodetector (TWPD) on semi-insulating (SI) InP substrate at 1.55 μm wavelength window with an electrical bandwidth of more than 120 GHz, a line characteristic impedance of about 50 Ω , and microwave index matched to the optical group index. The internal quantum efficiency more than 99% for a 200 μm long device is determined. The layer stack of the TWPD has previously utilized in a semiconductor optical amplifier (SOA). The TWPD can be monolithically integrated with passive and active components such as arrayed waveguide grating (AWG), Mach-Zehnder Interferometer (MZI), laser and modulator.

1. INTRODUCTION

The rapid expansion of optical communication networks has created requirement for increasing the capacity of such networks. TWPDs are key components in broadband receivers in which they provide easy, low cost and flexible photonic circuit design with maintaining high efficiency and broad bandwidth [1–5]. The ability of monolithic integration of the pin-TWPD with other passive and active devices such as AWG, modulator, and SOA makes it interesting for the researchers.

Received 5 February 2012, Accepted 6 April 2012, Scheduled 18 April 2012

* Corresponding author: Mahmoud Nikoufard (mnik@kashanu.ac.ir).

The pin-TWPD has a structure similar to the waveguide photodetector (WGPD) in which transparent cladding layers surround the absorbing non-intentionally doped guiding layer and the illumination is guided perpendicular to the carrier drift field. The WGPD suffers from a large mismatch between the photodetector and the load. To overcome the bandwidth limitation of the WGPD due to parasitic elements of the capacitance of junction area and the resistance of bulk semiconductors, the TWPD has been proposed [1]. In spite of the WGPD, the TWPD has special electrodes designed to support a traveling electrical wave with characteristic impedance that is matched to the external load. A TWPD is an in-plane device, consisting of two parts of the microwave waveguide and the optical part in which microwave and optical group velocities are matched. So, the TWPD can be electrically and optically modeled by a matched section of transmission line with an exponentially decaying photocurrent source propagating on it at the optical group velocity. In addition, the TWPD can arbitrarily be made long enough for nearly 100% internal quantum efficiency without compromising bandwidth [1].

Giboney et al. [1] modeled and realized a TWPD with 170 GHz bandwidth and about 50% quantum efficiency based on GaAs material. Beling et al. [4] reported a periodic parallel-fed TWPD monolithically integrated optical power splitter for high-speed (80 Gbit/s) and high-power applications. Recently, several high-speed traveling-wave uni-traveling carrier (UTC) photodetectors are demonstrated [5,6] but their structures are not suitable to monolithically integrate with other active and passive components. In current article, we analyzed a pin-TWPD which its layer stack has previously utilized in a SOA on highly doped n-InP substrate [8]. Then, this layer stack has used to realize a 40 GHz Mach-Zehnder interferometer (MZI)-based traveling-wave modulator [13,15]. In this paper, we changed the layer thicknesses and the ridge width of the MZI-modulator to reach a higher bandwidth while keeping the capability of monolithic integration with passive and active components such as AWG, SOA, and laser [13].

2. DEVICE STRUCTURE

The structure of the pin-TWPD with the doping level of layers is shown in Figure 1. The optical waveguide is formed by an absorbing non-intentionally doped InGaAsP layer with a wavelength cutoff bandgap of $1.55\ \mu\text{m}$ ($i\text{-}Q$ (1.55)) surrounded by the two $i\text{-}Q$ (1.25) layers to decrease the barrier height, to increase the optical confinement, and their bandgap is sufficiently far from the band edge of the operating wavelength at $1.55\ \mu\text{m}$. Using bulk $i\text{-}Q$ (1.55) instead of

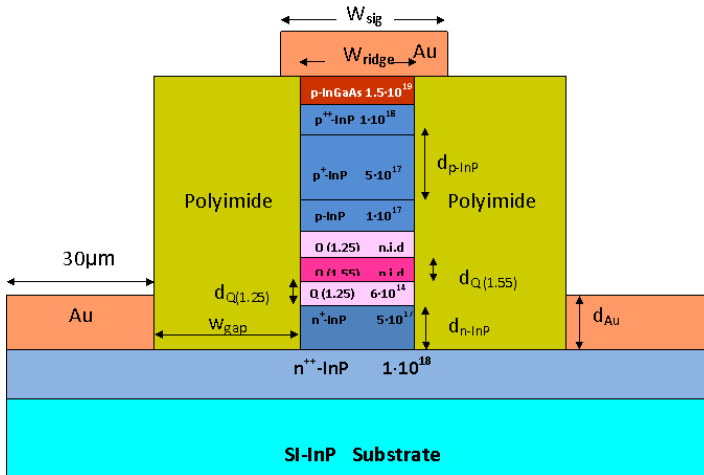


Figure 1. Schematic cross-section of the TWPD used in the electrical designs with the doping level of layers.

the multi-quantum well (MQW) materials offers the advantage of the polarization independent device [7]. The three *p*-doped cladding layers and the two buffer layers are from InP material with a graded doping level to reduce the optical loss and to make a low resistance path for carriers. A highly *p*-doped InGaAs layer with a thickness of 300 nm on top of the *p*-InP cladding layers is employed to form a low-resistance ohmic *p*-contact [13]. To achieve higher radio frequency (RF) bandwidth, a semi-insulating (SI) substrate is used to reduce the RF attenuation and the parasitic capacitance of the RF-probe and provides a good electric isolation of the components [7]. The polyimide is used to support a broader signal electrode respect to the ridge. The applied reverse bias voltage across the pin-structure sweeps the electron-hole pairs from the depleted region toward the electrodes.

3. SIMULATION RESULTS

3.1. DC-analysis

The DC-electrical simulations is carried out by utilizing a commercial numerical simulator (ATLAS/BLAZE) from Silvaco International (Silvaco ATLAS 2002), which solves the continuity and Poisson equations via finite element method (FEM). The transport of the generated carriers in the depletion region depends on the carrier density, carrier velocity and the magnitude of the local electric field.

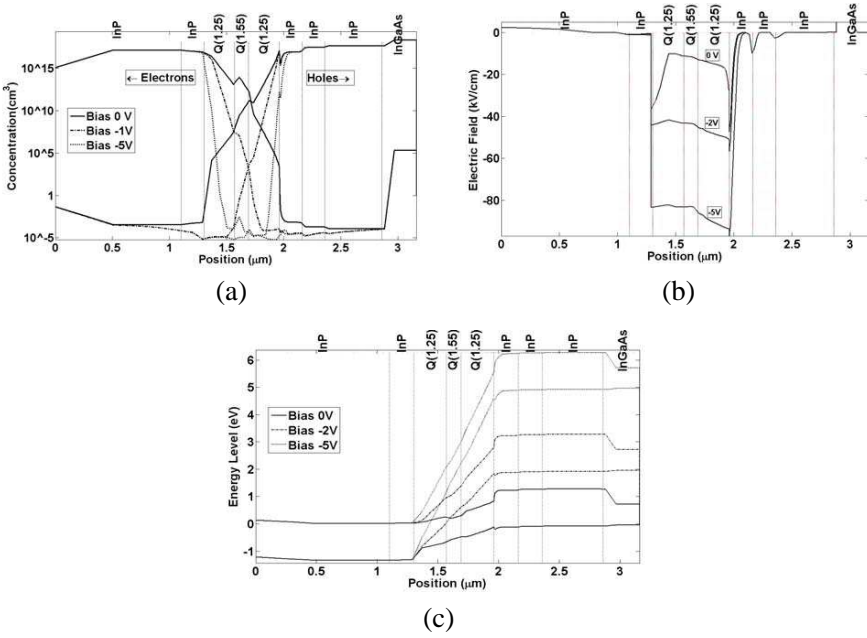


Figure 2. (a) Concentration of the electrons and holes, (b) electric field, and (c) band diagrams for three bias voltages of 0, -2 and -5 V.

The carrier density is related to the incident optical power, the carrier velocity is concerned to the applied electric field across the depletion layer, and the electric field strength depends on the location of the p-n-junction and the position of the heterostructure [11].

The operation of the TWPD was analysed by looking at the energy band diagrams, electric fields and doping concentrations at 0, 2 and 5 V reverse bias as shown in Figure 2. It shows that by applying 5 V reverse bias, the absorption layer of Q (1.55) and some parts of adjacent quaternary layers are depleted. The electrical field is related to the bending of the conductance band. The valence and conduction bands show a strong bending at the heterojunction as a result of the large bandgap difference between InP/InGaAsP materials. The bandgap offsets lead to high electric fields, depletion and pile-up of carriers at the heterojunctions as shown in Figure 2 [16].

The internal quantum efficiency is determined as $\eta_{int} = 1 - \exp(-\Gamma\alpha l)$ in which Γ , α and l are the confinement factor, the absorption coefficient and the length of the absorption layer of Q (1.55), respectively. In Ref. [9], we reported $\Gamma\alpha \approx 250/\text{cm}$ for a 120 nm thick Q (1.55) material. So, an internal quantum efficiency of more than

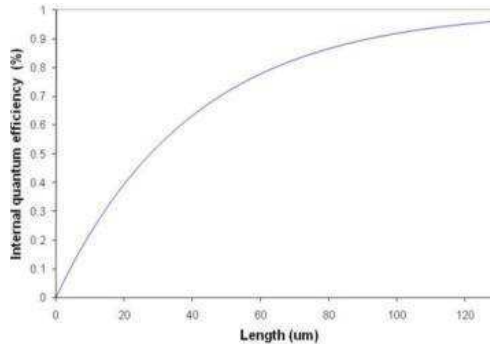


Figure 3. Internal quantum efficiency vs. length of the WGPD.

99% for a 200 μm long device is achievable (see Figure 3). In Ref. [7], a Waveguide photodetector is utilized with the same absorption layer thickness and was measured an internal efficiency about 90% for 80 μm long device. So, for 200 μm long device, our calculation is correct.

3.2. RF-analysis

Based on the relations available in [13], which determine the RF-bandwidth of a traveling-wave modulator, we extracted the similar relations for a TWPD as following: The RF-bandwidth of the TWPD can be defined as the generated RF-current, $I_{out}(f_{RF})$, to the static photocurrent, $I_{out}(f_0)$, as:

$$B(f_{RF}) = 20 \log \left(\frac{I_{out}(f_{RF})}{I_{out}(f_0)} \right) \tag{1}$$

where f_{RF} is the microwave frequency, and $f_0 \approx 0$ Hz is the frequency at direct current (DC). If the sinusoidal modulated optical carrier is launched to the photodetector, the two current density component of the bias current density, J_{DC} , and the single RF-tone current density with amplitude J_{RF} generated at $z = 0$ traveling at z -direction as:

$$J(f_{RF}, z) = J_{DC} + J_{RF} \exp(-(\alpha_{\mu} + jb)z) \tag{2}$$

For a TWPD with a reverse bias, the magnitude of the DC photocurrent is higher than the magnitude of the generated RF-photocurrent and the microwave attenuation α_{μ} depends on the microwave frequency. The walk-off parameter b accounting for the velocity mismatch between the two co-propagating, interacting field:

$$b = \frac{2\pi f_{RF}}{c} (n_{RF} - n_0) \tag{3}$$

where $n_{RF} = c/v_{RF}$ is the microwave index and $n_0 = c/v_0$ is the optical group index. The normalized photocurrent amplitude response $|A|$ can then be obtained by integrating Eq. (2) over z :

$$|A| = 20 \log \left| \frac{1}{L} \int_0^L \exp(-(\alpha_\mu + jb)z) dz \right| = 20 \log \left| \frac{1 - \exp(-(\alpha_\mu + jb)L)}{L(\alpha_\mu + jb)} \right|$$

$$= 20 \log \frac{\sqrt{\exp(-2\alpha_\mu L - 2 \exp(-\alpha_\mu L) \cos(bL)) + 1}}{L \sqrt{\alpha_\mu^2 + b^2}} \quad (4)$$

The photodetector bandwidth of 3 dBe corresponds to a reduction of 1.5 dBo in optical power or a reduction of $1/\sqrt{2}$. Thus, in a velocity-matched situation ($b = 0$), the 3 dBe bandwidth is reached when the photocurrent over the total photodetector length L has dropped by:

$$\frac{1}{\sqrt{2}} = \frac{1 - \exp(-\alpha_\mu L)}{\alpha_\mu L} \quad (5)$$

So we have $\alpha_\mu L \approx 0.738 \text{ Np} = 6.41 \text{ dBe}$ i.e., the electrical bandwidth of the photodetector is at microwave attenuation of 6.41 dBe. Each semiconductor layer and lossy metallic electrodes have the finite resistivity and influence the RF-attenuation and can be considered by means of complex dielectric constant, $\epsilon_r = \epsilon'_r + j\epsilon''_r = n^2$. For both InP and InGaAsP materials, the real part of the relative permittivity (ϵ'_r) is assumed 3.54 [13, 14] and the imaginary part is evaluated using

$$\epsilon''_r = -\frac{\sigma}{2\pi f \epsilon_0} \quad (6)$$

In which the conductivity σ is given by

$$\sigma = e(\mu_e n + \mu_p p) \quad (7)$$

n and p denote the doping concentration for n - and p -doped material, respectively; e is the electron charge; μ_e and μ_p are the mobility of electron and holes at n - and p -doped materials, respectively. The metallic loss is determined as

$$\epsilon_r = -j \frac{\sigma}{2\pi f \epsilon_0} \quad (8)$$

ϵ_0 is the vacuum permittivity.

The TWPD has been simulated at RF frequencies by using the Ansoft HFSS software according to the cross-section presented in Figure 1. The initial values of the layer thickness of the TWPD are chosen as described in Ref. [13]: The absorbing layer and two adjacent layers have a thickness of 190 nm, 120 nm, 120 nm, respectively. The

cladding and buffer layers with a total thickness of 1000 nm and 1000 nm, respectively. We have also considered a ridge width of 1000 nm, a signal line width of 2000 nm, a signal and electrode gold thickness of 1000 nm, and signal-ground gap of 8 μm . With this layer stack, the obtained results are also compared with the simulation and measurement results given in [13].

Three design parameters of the TWPD are the line impedance, microwave index and microwave attenuation. The three main parameters which determine the microwave loss and index are the ridge width, the gold thickness and the signal line width. A smaller ridge width reduces the microwave loss and the low doping levels of the cladding layers increases microwave loss. A thinner ridge also reduces index and the line impedance but the minimum ridge width is restricted by the fabrication technology and the optical field can be in the cutoff mode. The minimum ridge width is about 750 nm in which by reducing the ridge width, the optical field will be in cutoff mode. The impedance depends on the ridge width, the signal line width, the electrode thickness, the layer thickness and doping, and the gap between the signal and ground electrodes. The effect of the shape of the signal electrode show that a wide and thick signal line reduces the RF propagation loss, because of the skin depth of gold and a large part of the electric field is in the air instead of the ridge, respectively. A larger gap increases the microwave attenuation due to increasing the carrier path, so increases the resistivity of the n -bulk material. The p - and n -cladding thickness and doping level have little effect on the microwave index and impedance. The minimum thickness of the p -cladding layer is needed to keep the tail of the optical field far from the highly doped InGaAs contact layer to reduce the optical attenuation for long device. Calculation shows that 95% of the optical field is confined in a region that extends 200 nm on both sides of the waveguide layers. By keeping the first 200 nm of the cladding layers adjacent to the waveguide layers

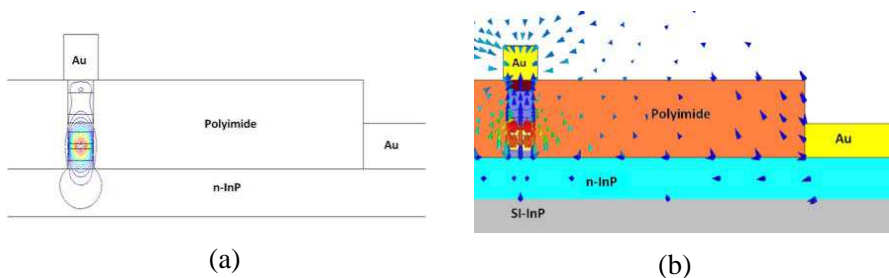


Figure 4. (a) Optical analysis, and (b) microwave electric field in the cross-section of the TWPD. In the film layers of i -Q (1.55) and i -Q (1.25), the optical field and the electrical field have maximum values.

with a low doping level, the optical loss is very low [7]. Next 700 nm cladding thickness is graded doped to have low optical loss and low resistance, whereas it is sufficient for keeping the losses negligible in the top InGaAs layer.

In this design, the thickness of the absorbing i -Q (1.55) layer and two adjacent i -Q (1.25) layers have been chosen equal to 120 nm, 270 nm and 270 nm, respectively, the cladding and buffer layers with a total thickness of 900 nm and 1300 nm, respectively, the ridge width of

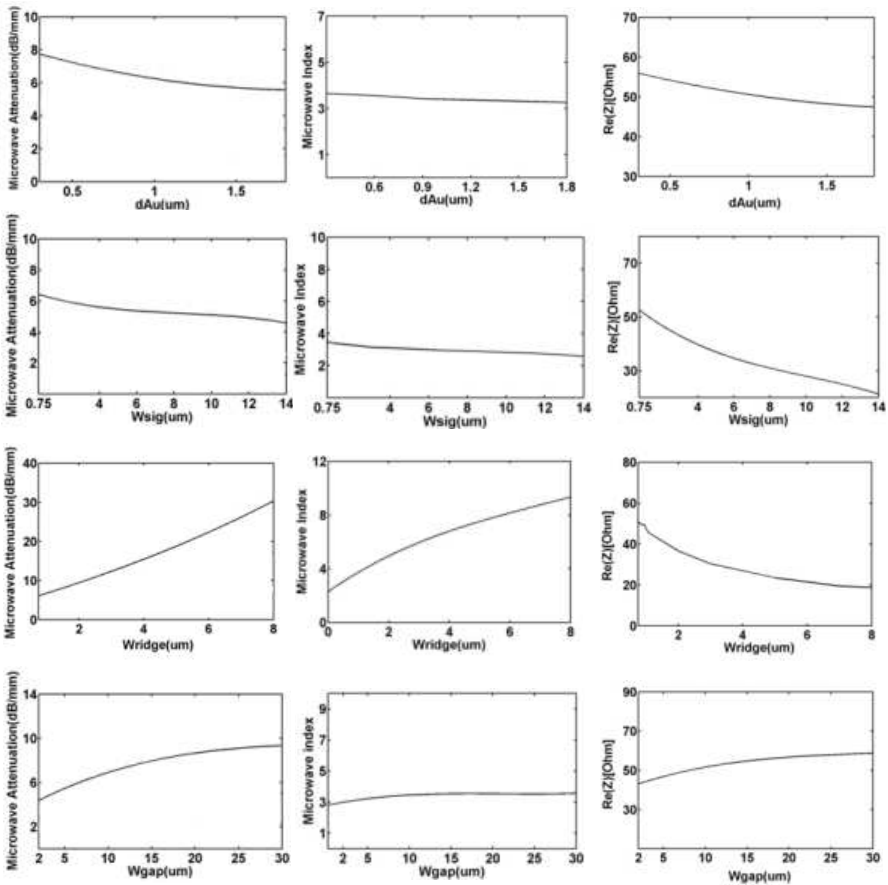


Figure 5. Microwave attenuation, microwave index and real and imaginary parts of impedance simulated at 120 GHz as a function of gold thickness, gap width, signal line width, and ridge width. For each plot, the parameters that are kept constant are as mentioned on Section 2.

750 nm, the signal line width of 1000 nm, the signal and electrode gold thickness of 1000 nm, and the signal-ground gap of $8\ \mu\text{m}$. The above layer stack is chosen as a compromise between main three parameters of line impedance, microwave index, and microwave attenuation by trial and error through simulations. The optical and electrical field distribution is presented in Figure 4 and shows that the maximum optical and electrical field intensity is inside the depleted waveguide layers of Q (1.55) and Q (1.25). Due to high conductivity of the n-InP buffer layer with a doping level of $1e18/\text{cm}^3$, the mode is nearly microstrip [15].

Figure 5 demonstrates the microwave attenuation, microwave index and real part of the impedance simulated at 120 GHz frequency as a function of gold thickness d_{Au} , signal electrode width W_{sig} , ridge width W_{ridge} , and gap between the signal and the ground electrode W_{gap} , respectively. For each plot, the rest parameters are kept constant as mentioned above.

Based on nearly optimized values of the TWPD, the microwave loss and index are determined (see Figure 6). The optical group index is calculated about 3.62 by using COMSOL software. Since, the simulated microwave index is very close to the optical group index, the RF-bandwidth of the TWPD will be limited by the microwave attenuation which shows an electrical bandwidth of more than 120 GHz. The characteristic impedance of the TWPD should be matched to the load impedance of $50\ \Omega$. The characteristic impedance can be determined by using the simulated S -parameters of device. The real and imaginary parts of the characteristic impedances of the TWPD are about $50\ \Omega$ and $0\ \Omega$ at frequencies over 20 GHz as shown in Figure 6.

In addition, one of the bandwidth limitations of the TWPD is charge trapping in the hetero-junctions. When electron-hole pairs that are generated in the depletion region, travel towards the contact

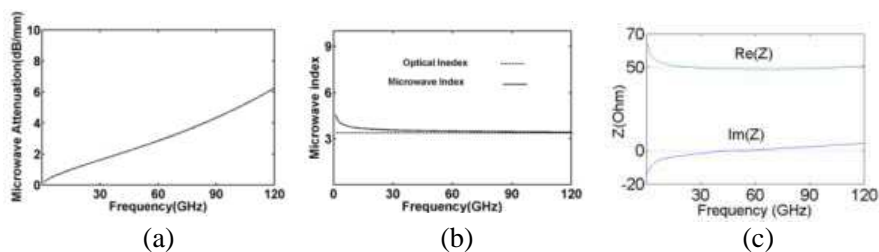


Figure 6. (a) Microwave attenuation, (b) microwave index, and (c) real and imaginary parts of the characteristic impedance of the TWPD versus frequency up to 120 GHz.

layers, they can be trapped in the barriers of the double heterostructures. Charge trapping causes recombination of electron and holes in heterostructure junctions and decreases the speed of carriers traveling toward electrodes. For this reason, a p -Q (1.25) layer with an wavelength bandgap of 1.25 μm is placed between i -InGaAsP absorption layer with an wavelength bandgap of 1.55 μm and p - and n -InP (the wavelength bandgap of 0.92 μm) cladding layers to reduce the effects of the barriers. In the Ref. [17], the charge trapping effect on the bandwidth limitation for the pin-WGPD based on an InP/InGaAsP layer stack has been neglected.

4. CONCLUSION

In this article, we analysed a TWPD structure based on a semiconductor optical amplifier/laser layer stack. It is tried to reduce the microwave attenuation, to match the microwave index and the optical group index, matching the characteristic impedance to 50 Ω by obtaining the width of ridge and signal electrode and the thickness of the i -Q (1.25) and i -Q (1.55) film layers. The device shows the 6.41 dB bandwidth of more than 120 GHz, the line impedance of about 50 Ω , and the microwave refractive index close to optical refractive index of 3.62. We also determined an internal quantum efficiency of about 99% for 200 μm long device.

REFERENCES

1. Giboney, K. S., J. W. Rodwell, and J. E. Bowers, "Traveling-wave photodetector theory," *IEEE Trans. Microwave Theory Tech.*, Vol. 45, No. 8, 1310–1319, 1997.
2. Pasalic, D. and R. Vahldieck, "A hybrid drift-diffusion-TLM analysis of traveling-wave photodetectors," *IEEE Trans. Microwave Theory Tech.*, Vol. 53, No. 9, 2700–2706, 2005.
3. Torrese, G., "Ultra-wide bandwidth photodetectors for optical receivers," Ph.D. Dissertation, Universite Catholique De Louvain, 2002.
4. Beling, A., J. C. Campbell, H. G. Bach, G. G. Mekonnen, and D. Schmidt, "Parallel-fed traveling wave photodetector for > 100-GHz applications," *IEEE J. Lightw. Technol.*, Vol. 26, No. 1, 16–20, 2008.
5. Rouvalis, E., C. C. Renaud, D. G. Moodie, M. J. Robertson, and A. J. Seeds, "Traveling-wave uni-traveling carrier photodiodes for

- continuous wave THz generation,” *Opt. Express*, Vol. 18, No. 11, 11105–11110, 2010.
6. Zhang, Y. X., J. Q. Pan, L. J. Zhao, H. L. Zhu, and W. Wang, “Design and characterization of evanescently coupled uni-traveling carrier photodiodes with a multimode diluted waveguide structure,” *Chin. Phys. Lett.*, Vol. 27, No. 2, 028501, 2010.
 7. Xu, L., M. Nikoufard, X. J. M. Leijtens, T. de Vries, E. Smalbrugge, R. Notzel, Y. S. Oei, and M. K. Smit, “High-performance InP-based photodetector in an amplifier layer stack on semi-insulating substrate,” *IEEE Photon. Technol. Lett.*, Vol. 20, No. 23, 1941–1943, 2008.
 8. Smit, M. K. and R. G. Broeke, “A wavelength converter with integrated tunable laser,” *Integr. Photon. Res. (IPR '03)*, paper IMB4, Washington, 2003.
 9. Nikoufard, M., “Integrated wavelength division multiplexing receivers,” Ph.D. Dissertation, Eindhoven University of Technology, 2008.
 10. Silvaco ATLAS, *User's Manual*, SILVACO International, 2002.
 11. Steenbergen, C. A. M., “High capacity integrated optical receivers,” Ph.D. Dissertation, Eindhoven University of Technology, 1997.
 12. De Paola, F. M., V. D'Alessandro, A. Irace, J. H. den Besten, and M. K. Smit, “Novel optoelectronic simulation strategy of an ultrafast InP/InGaAsP modulator,” *Optics Communications*, Vol. 256, 326–332, 2005.
 13. Den Besten, J. H., “Integration of multiwavelength lasers with fast electro-optical modulator,” Ph.D. Dissertation, Eindhoven University of Technology, 2004.
 14. EMIS Data reviews Series No. 6, *Properties of Indium Phosphide*, INSPEC, 1991.
 15. Pascher, W., J. den Besten, D. Caprioli, R. van Dijk, X. J. M. Leijtens, and M. K. Smit, “Modelling and characterization of a travelling-wave electro-optic modulator on InP,” *Advances in Radio Science*, Vol. 1, 67–71, 2003.
 16. Nikoufard, M. and S. N. Ghafouri, “Symmetric twin-waveguide photodetector on semi-insulating InP substrate at 1.55 μm wavelength,” *Journal of Optics*, Vol. 13, 055502, 2011.
 17. Alping, A., “Waveguide pin photodetectors: Theoretical analysis and design criteria,” *IEE J. of Optoelectronics*, Vol. 136, No. 3, 177–182, 1989.